ACS Photonics

Letter

Cite This: ACS Photonics 2019, 6, 600−604

pubs.acs.org/journal/apchd5



# Spatiotemporal Analysis of an Efficient Fresnel Grating Coupler for Focusing Surface Plasmon Polaritons

Daniel Podbiel,*,† Philip Kahl,† Bettina Frank,‡ Timothy J. Davis,§ Harald Giessen,‡ Michael Horn-von Hoegen,† and Frank J. Meyer zu Heringdorf*,†

†Faculty of Physics and CENIDE, University of Duisburg-Essen, 47057 Duisburg, Germany

‡Fourth Physics Institute and Research Center SCoPE, University of Stuttgart, 70550 Stuttgart, Germany

§School of Physics, University of Melbourne, Parkville Victoria 3010, Australia

**ABSTRACT:** Time-resolved photoemission microscopy is used to investigate the spatiotemporal properties of surface plasmon polaritons launched at a Fresnel-type grating coupler. By milling a multiline structure of segmented grooves with dimensions derived from Fresnel zones into a plasmonic material, efficient focusing of surface plasmon polaritons can be accomplished. We demonstrate the presence of pulse broadening at the focus associated with propagation delays in the device. Moreover, our experimental data implies an enhancement of the plasmonic field energy density at the focus in excess of a factor of 10, with a focal spot size at the Abbe limit for our lens.

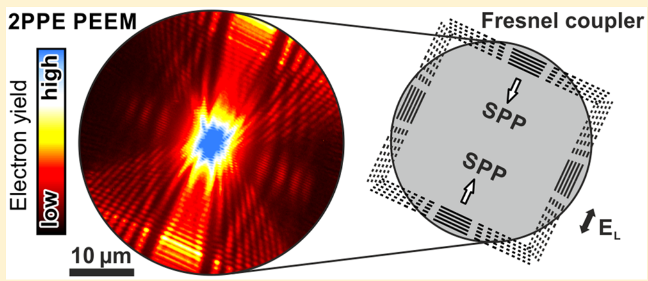


**KEYWORDS:** *Time-resolved photoemission microscopy, plasmoemission, two photon photoemission, surface plasmon imaging*

Surface plasmon polaritons (SPPs) have been suggested as a possible pathway for surpassing the diffraction limit of photonic devices.[1−3] Accordingly, concepts for converting and guiding light in plasmonic structures[4,5] as well as utilizing plasmons to concentrate light[6] have been heavily researched during the last years. Because of their wavenumber mismatch to propagating light in vacuum, initiating SPPs on metal surfaces can be problematic. It is well-known that diffraction gratings can provide additional momentum to the incident light, enabling strong coupling into surface plasmon waves.[7−10] Diffraction of the SPPs themselves is also possible, allowing focusing from an array of opaque stripes that form a Fresnel grating.[11,12] The Fresnel grating represents a particular solution to the holographic problem of designing a diffracting structure to create a desired SPP beam.[13] SPP focusing can be combined with coupling, as observed when using scattering centers arrayed in an arc[14] as well as from a curved diffraction grating.[15]

Here we combine the functionality of exciting SPPs and focusing them with an optimized multiline Fresnel-coupling structure in extension of the work by Schneider and Lemke.[16,17] Particularly, we analyze the spatiotemporal focusing properties of the lens with femtosecond time resolution using normal-incidence time-resolved two-photon photoemission (2PPE) combined with photoemission electron microscopy (PEEM).[18,19]

The Fresnel-type grating coupler consists of a series of slits milled into the metal surface so that the electric field of the incident light generates surface charge excitations that propagate away as SPPs. The design is based on Huygens' principle, as illustrated in Figure 1a. The coupler is mirror-symmetric around the vertical dashed-dotted black line, so that we need only highlight one-half (the right side) of the coupler, although some phase-fronts of SPPs excited at the left side of the coupler are also indicated. To focus SPPs into a focal point F, several segmented lines (the horizontal black lines in Figure 1a) are milled into the metal surface so that all excited SPPs interfere constructively at focus F. Locations on the surface where excited SPPs would cause destructive interference at the focal point are not milled, and at these locations SPPs are not excited.

For each of the segmented lines $i$ in Figure 1a that constitute the grating coupler, the concept is mathematically equivalent to focusing a plane light wave with a partly transparent Fresnel zone plate.[20] In such zone plates, focusing of a plane light wave into a focal point a distance $f$ from the lens occurs when the zones switch from opaque to transparent at coordinates

$$r_n = \pm(n\lambda f + n^2\lambda^2/4)^{1/2} \tag{1}$$

with the zone index $n \geq 0$. In our case, the zones of the innermost lines of the coupler were calculated with $\lambda = \lambda_S = 780$ nm for the SPP wavelength and $f_0 = 16.88$ $\mu$m for the focal length. Instead of being opaque or transparent, however, the zones are distinguished by their capability to excite SPPs (or not). Accordingly, the $r_n$ denote the beginning and end of the line segments milled as slots into the metal surface using a focused ion beam (FIB). For the focusing properties, it is not important if the lines start at an even $n$ and end at an odd $n$ or vice versa,

Received: November 13, 2018
Published: February 21, 2019

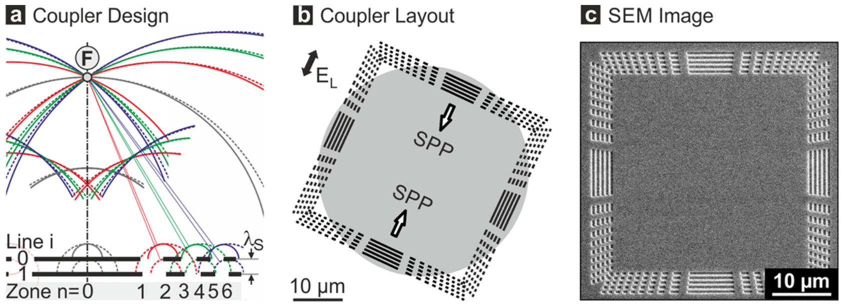


**Figure 1.** Fresnel-type grating couplers for focusing of surface plasmon polaritons. (a) Design of a grating coupler consisting of $i$ segmented excitation lines spaced by the SPP wavelength $\lambda_S$. The segmentation of each line has been calculated individually to resemble $n$ Fresnel zones and to form a focus at F. (b) Sketch of the advanced grating coupler arrangement investigated in this study. Two pairs of two opposing grating couplers are rotated by 90° with respect to each other. The polarization of the laser pulses is adjusted for excitation of SPPs at the indicated couplers. The field of view in Figure 2 is indicated in gray. (c) Scanning electron micrograph of the focused ion beam milled grating coupler sketched in panel (b) on a single crystalline Au platelet.

since exchanging milled and unmilled areas only introduces a SPP phase-shift of $\varphi_0 = \pi$ at the focal point. Just like an optical zone plate, our Fresnel-type grating coupler exhibits substantial chromatic aberration and will work best for narrow-band SPP wavepackets or monochromatic SPP waves.

To increase the coupling efficiency, we use five segmented lines shifted by one SPP wavelength $\lambda_S$ with respect to each other. Since the distance between each line $i$ of the grating coupler and the desired focal point at F is different, the segmentation of each line within the coupler has to be calculated individually to yield a focal length $f_i = f_0 + i\cdot\lambda_S$. Accordingly, due to the square-root dependence $r_n(f)$, the segments of lines further away from the focus point must be larger, as is clearly visible in Figure 1. Introducing additional segments in this fashion also biases the scattering into one direction toward the focus, since SPPs propagating outward from the segments no longer obey the phase-matching condition and do not form a focal point.

To further improve the SPP field strength at the focal point, we simultaneously use two opposing Fresnel-type grating couplers, where one is the mirror image of the other. The distance of the couplers is simply twice their focal length. Figure 1b shows the resulting Fresnel-coupler layout that was milled into the sample. The black lines indicate FIB cuts, and the filled gray circle marks the field of view used for 2PPE PEEM imaging in Figure 2. Each Fresnel-type coupler consists of five segmented lines. Moreover, four couplers were structured in rotational increments of 90° with respect to each other. Figure 1c shows a scanning electron micrograph of the grating coupler structure, FIB milled into a single-crystalline Au platelet.

The experiments were performed in a spectroscopic photoemission low energy electron microscope (SPE-LEEM III, Elmitec GmbH). The ultrahigh vacuum microscope with a base pressure below $1 \times 10^{-10}$ mbar is combined with a pulsed Ti:sapphire laser oscillator (Femtolasers) for nonlinear and time-resolved photoemission measurements of SPP propagation. The fundamental wavelength of the laser pulses was 800 nm, with a spectral full width at half-maximum (fwhm) of approximately 75 nm, and a pulse duration of <20 fs. Details of the experimental setup have been described in previous work.[18,21,22]

The 2PPE PEEM method[23] has been established as a particularly suitable technique for efficient imaging of SPPs with nanometer resolution.[24−27] The recent development of normal illumination has enabled full imaging of the temporal dynamics of SPP waves[18,19] in a variety of nanoplasmonic applications.[28,29] Here we use this technique to measure the field enhancement at the focal point of the planar Fresnel coupler as well as image the phase delays associated with SPPs arriving from distant elements in the grating.

Single-crystalline atomically flat Au platelets, fabricated by a single step thermolysis of a $(AuCl_4)$−tetraoctylammonium complex on the native oxide layer of a Si substrate[30] were used as plasmonic samples. The grating couplers used for excitation of SPPs were milled into the platelets by ex situ focused ion beam (FIB) milling. Prior to the measurements, a submonolayer amount of Cs was deposited onto the sample from a standard Cs dispenser (SAES Getters) to reduce the work function and enable a 2PPE process.

We obtain a time-resolved visualization of SPP propagation in a normal-incidence geometry by a pump−probe scheme, where pairs of mutually delayed laser pulses impinge on the surface along the surface normal.[19] Figure 2a,c show two time-resolved 2PPE PEEM images in a logarithmically scaled false-color representation acquired at different delays $\Delta t$ between the laser pulses. The polarization of the laser pulses is parallel to the surface plane and has been adjusted to only excite SPPs at the top-right and bottom-left grating couplers. The measured 2PPE PEEM yield is given by the time-integrated photoemission signal that is formed by the superposition of the laser and the SPPs' electromagnetic fields.

Figure 2a shows the electron yield at zero pump−probe delay, $\Delta t = 0$. The fringes with a spatial periodicity of $\lambda_S$ in the vicinity of the grating coupler result from the interference of the electric field of the laser pulse with the field of the excited SPP waves.[18,21] All other signatures and the contrast present in the image originate exclusively from plasmoemission, that is, the decay of SPP to single electron excitations, and the subsequent emission of the excited electrons in the absence of light.[21,31,32] The pronounced electron yield at the focal point is also exclusively due to plasmoemission. A close inspection of the focal point reveals that the periodicity of the interferometric correlation pattern at the focus resembles $\lambda_S/2$. This half-wavelength observation is due to the formation of a transient standing wave by the counter-propagating SPP pulses[31] from the opposing grating couplers.

To investigate the spatiotemporal properties of the SPP propagation, in Figure 2b profiles across the 2PPE PEEM images were extracted for different delay times and assembled into a color-scale image plot. High-dynamic-range techniques for local



DOI: 10.1021/acsphotonics.8b01565
ACS Photonics 2019, 6, 600−604

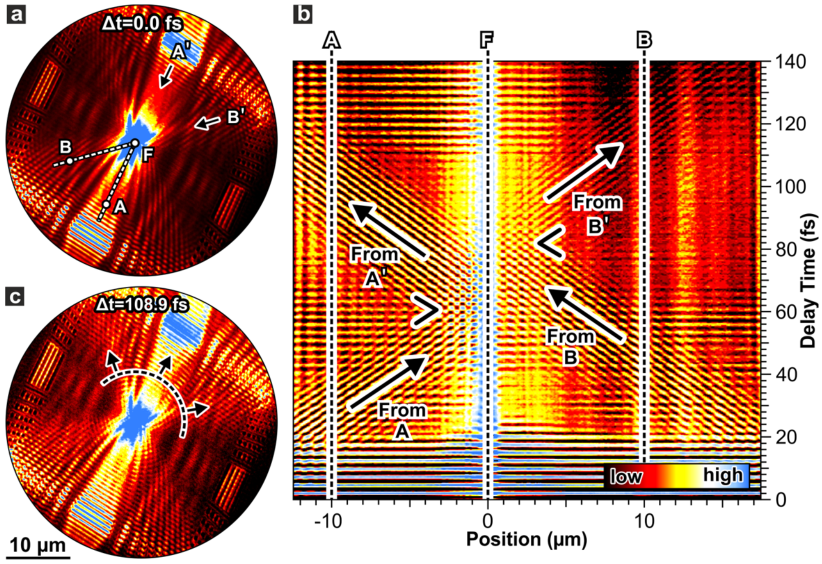


**Figure 2.** Spatiotemporal analysis of the Fresnel-type coupler's focusing properties. (a) Logarithmically scaled false color representation of the 2PPE PEEM electron yield measured at zero pump−probe delay time. The contrast in the vicinity of the focus is predominantly due to plasmoemission. (b) Temporal dynamics of SPP propagation, extracted from a time-resolved measurement. The sections were extracted along lines A−F and F−B in panel (a) showing the time/phase delay associated with SPP pulses originating from different regions on the Fresnel grating. The image has been optimized by high-dynamic-range local-contrast enhancement techniques to emphasize the propagating phasefronts, and the color scale is quantitatively different from the one in the other two panels. (c) Logarithmically scaled false color representation of the 2PPE PEEM electron yield measured at a delay time $\Delta t = 108.9$ fs, highlighting the formation of concentric SPP wavefronts diverging from the focus. The slight overall intensity gradient from the top right to the lower left in panels (a) and (c) is due to a slight mis-centering of the laser on the grating coupler, amplified by the nonlinear nature of the emission process and the logarithmic scaling.

contrast enhancement were applied to emphasize the weaker interference signals over the strong plasmoemission at the focus point (with the consequence that the color scales of Figure 2a,c are not quantitatively comparable to the color scale in Figure 2b). The path of each extracted profile is indicated in panel (a) and characteristic points are marked. The lower two arrows in Figure 2b each indicate a femtosecond SPP pulse that is launched at time $\Delta t = 0$ fs at a particular segment of the grating coupler and propagates through points A or B toward the focal point in F. Points A and B were chosen to be equidistant from the focal point and their positions are marked by vertical lines in Figure 2b. The vertical line at position F marks the delay-time-independent plasmoemission signature at the focus. The bright diagonal lines (in the vicinity of the arrows) indicate trajectories of constant phase of the wavefronts as a function of delay-time, and the slope of these lines corresponds to the phase velocity of the SPP. The SPP pulses propagating through points A and B toward the focus are clearly visible, and the pulse from A arrives at the focus point at a delay-time between 50−70 fs. At larger delay times, phasefronts moving away from the focus are visible in panel (b) as well. These originate from the opposite coupler and indicate pulses from A′ and B′ that crossed through the focus point.

The SPP pulse passing through point A arrives at the focal point earlier than the pulse passing through point B, originating from the corner of the grating coupler. More specifically, the SPP pulse passing through B is excited at line segment 8, that is, it comes from the FIB-milled groove between the Fresnel zones 16 and 17, using the indexing of the Fresnel zones as introduced in Figure 1a. The two wave trains become separated in time because the SPP waves excited at higher-order Fresnel zone segments must travel further to the common focal point than the SPP waves excited at grooves corresponding to lower order Fresnel zones. More specifically, the phase fronts passing through B arrive at the focus 8 optical cycles later than those passing through A. The time lag is highlighted by the two markers (> and <) in Figure 2b. These markers are placed at the symmetry points of the phase fronts from A−A′ and B−B′. The time difference between the markers is $\Delta t = 21.3$ fs, which corresponds to a delay of 8 phase fronts, consistent with the separation of the corresponding line segments in the Fresnel grating coupler. The superposed SPP pulse at the focal point is thus temporally broadened by ≈21 fs compared to the pulse close to the grating coupler. Additional features in the figure, such as the horizontal lines around 120 fs delay time, are not of importance here, but are explained by applying the spatiotemporal analysis of strong SPP waves in ref 31.

Figure 2c is a 2PPE PEEM image taken at a large time delay, after the pulses have passed through the focus. This figure illustrates how the coherent and constructive interference of the SPPs from different Fresnel zones results in spherical phase fronts. Indeed, our Fresnel grating coupler creates spherical phase fronts close to the focus, similar to a regular lens.

The SPP propagation and the 2PPE PEEM experiment were modeled using a wave-mechanical simulation code including plasmoemission[33] with the results shown in Figure 3a. The simulation takes account of the SPPs launched from a Fresnel grating coupler, the pulsed nature of the pump and probe signals, and the time integration inherent in the 2PPE PEEM method. Figure 3b compares the line profiles of the electron yield from the experimental data with the simulation. The experimental and simulation profiles, obtained along the dashed line in Figure 3a, show good agreement over almost 3 orders of magnitude in intensity. In the simulation, the only fitting parameter was the maximum yield of the simulated profile. From the experiment, we compare the 2PPE PEEM yield at the focal point with the 2PPE PEEM yield from the plasmoemission background and find a ratio of approximately 10000:50, which corresponds to an


DOI: 10.1021/acsphotonics.8b01565
ACS Photonics 2019, 6, 600−604

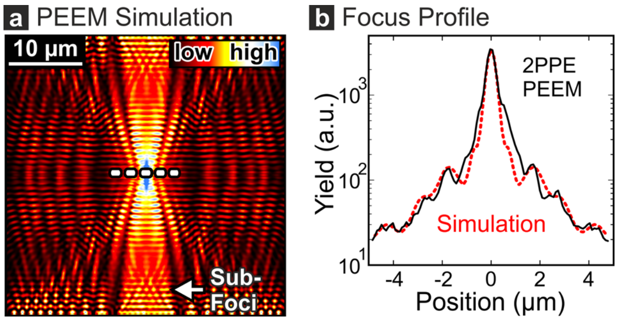


**Figure 3.** (a) Simulation of the 2PPE PEEM image of the Fresnel grating coupler with pump−probe delay time $\Delta t = 0$ fs. The contrast is predominantly due to plasmoemission; (b) the electron yield for a section through the focal point, comparing simulation with experiment.

enhancement of SPPs electromagnetic field energy density of approximately $\sqrt{10000:50} \approx 14$. The central focal spot has a fwhm of 440 nm for the 2PPE signal, which depends on the square of the plasmon intensity $I_p^2$ so that the fwhm of the SPP focus is 660 nm, being about $\sqrt{2}$ larger. This is consistent with the Abbe diffraction limit for our lens of numerical aperture NA = 0.58, which gives $\lambda_p/2\text{NA} = 670$ nm.

The typical subfoci formed by zone plates at positions $f/(2j + 1), j > 1$[20] are weak in Figures 2 and 3 compared to the focus at F, since the focal lengths and thus the positions of the subfoci are at different positions for each of the shifted segmented lines. Only in the focal point at F is there complete constructive interference of the SPP waves of all grating couplers.

Any SPP-based nano-optical device will require efficient coupling of light into SPPs with, potentially, subsequent focusing from the plasmonic far field into functional building blocks. Ideally, the coupling structures should be small, easy to fabricate, polarization sensitive, and support high switching frequencies. The optimized Fresnel couplers discussed here fulfill most of these requirements. Efficient focusing down to the Abbe limit was demonstrated using pairs of opposing grating couplers, each consisting of several segmented grooves with different focal lengths. In the focus point we find a >10-fold enhancement of the SPP field's energy density, demonstrating that the simultaneous coupling and focusing of SPPs can be achieved. The temporal broadening of the coupler by 21 fs is negligible compared to the usually desired switching frequencies in photonic or plasmonic devices in the THz range. Our work also highlights a limitation with such focusing devices when designed for ultrashort optical pulses and large focal lengths. Propagation delays between elements at different distances from the focal point can result in SPP pulses arriving at the focus at different times, thereby reducing the overall intensity there and broadening the focal spot due to incomplete phase cancellation in that region. These results illustrate the power of normal incidence 2PPE PEEM for in situ investigation of plasmonic devices in which SPPs propagate in different directions.

## AUTHOR INFORMATION


### Corresponding Authors

*E-mail: daniel.podbiel@uni-due.de.
*E-mail: meyerzh@uni-due.de.

### ORCID

Daniel Podbiel: 0000-0002-6592-4146
Timothy J. Davis: 0000-0002-7299-4900
Frank J. Meyer zu Heringdorf: 0000-0002-5878-2012


### Notes

The authors declare no competing financial interest.

## ACKNOWLEDGMENTS

Financial support from the Deutsche Forschungsgemeinschaft (DFG) through SFB 616 "Energy Dissipation at Surfaces", SPP 1391 "Ultrafast Nanooptics", and CRC 1242 "Non-Equilibrium Dynamics of Condensed Matter in the Time Domain" (Project No. 278162697-SFB 1242) as well as ERC (Complexplas), BMBF, Zeiss-Stiftung, and BW Stiftung is gratefully acknowledged.

## REFERENCES

(1) Ozbay, E. Plasmonics: merging photonics and electronics at nanoscale dimensions. *Science* **2006**, *311*, 189−193.
(2) Atwater, H. The promise of plasmonics. *Sci. Am.* **2007**, *296*, 56.
(3) Brongersma, M. L.; Shalaev, V. M. The case for plasmonics. *Science* **2010**, *328*, 440−441.
(4) Barnes, W. L.; Dereux, A.; Ebbesen, T. W. Surface plasmon subwavelength optics. *Nature* **2003**, *424*, 824−830.
(5) MacDonald, K. F.; Samson, Z. L.; Stockman, M. I.; Zheludev, N. I. Ultrafast active plasmonics: transmission and control of femtosecond plasmon signals. *Nat. Photonics* **2009**, *3*, 55−58.
(6) Schuller, J. A.; Taubner, T.; Brongersma, M. L. Optical antenna thermal emitters. *Nat. Photonics* **2009**, *3*, 658−661.
(7) Koev, S. T.; Agrawal, A.; Lezec, H. J.; Aksyuk, V. A. An Efficient large-area grating coupler for surface plasmon polaritons. *Plasmonics* **2012**, *7*, 269−277.
(8) Devaux, E.; Ebbesen, T. W.; Weeber, J.-C.; Dereux, A. Launching and decoupling surface plasmons via micro-gratings. *Appl. Phys. Lett.* **2003**, *83*, 4936−4938.
(9) Ditlbacher, H.; Krenn, J. R.; Hohenau, A.; Leitner, A.; Aussenegg, F. R. Efficiency of local light-plasmon coupling. *Appl. Phys. Lett.* **2003**, *83*, 3665−3669.
(10) Sheng, P.; Stepleman, R. S.; Sanda, P. N. Exact eigenfunctions for square-wave gratings: Application to diffraction and surface-plasmon calculations. *Phys. Rev. B: Condens. Matter Mater. Phys.* **1982**, *26*, 2907−2916.
(11) Fang, Z.; Lin, C.; Ma, R.; Huang, S.; Zhu, X.; Planar. Plasmonic focusing and optical transport using CdS nanoribbon. *ACS Nano* **2010**, *4*, 75−82.
(12) Feng, L.; Tetz, K. A.; Slutsky, B.; Lomakin, V.; Fainman, Y. Fourier plasmonics: Diffractive focusing of in-plane surface plasmon polariton waves. *Appl. Phys. Lett.* **2007**, *91*, 081101.
(13) Dolev, I.; Epstein, I.; Arie, A. Surface-plasmon holographic beam shaping. *Phys. Rev. Lett.* **2012**, *109*, 203903.
(14) Yin, L.; Vlasko-Vlasov, V. K.; Pearson, J.; Hiller, J. M.; Hua, J.; Welp, U.; Brown, D. E.; Kimball, C. W. Subwavelength focusing and guiding of surface plasmons. *Nano Lett.* **2005**, *5*, 1399−1402.
(15) Radko, I. P.; Bozhevolnyi, S. I.; Brucoli, G.; Martin-Moreno, L.; Garcia-Vidal, F. J.; Boltasseva, A. Efficient unidirectional ridge excitation of surface plasmons. *Opt. Express* **2009**, *17*, 7228−7232.
(16) Lemke, C.; Schneider, C.; Leißner, T.; Bayer, D.; Radke, J. W.; Fischer, A.; Melchior, P.; Evylukhin, A. B.; Chichkov, B. N.; Reinhardt, C.; Bauer, M.; Aeschlimann, M. Spatiotemporal characterization of SPP pulse propagation in two-dimensional plasmonic focusing devices. *Nano Lett.* **2013**, *13*, 1053−1058.
(17) Schneider, C. Mapping of surface plasmon polariton fields by time-resolved photoemission electron microscopy: Experiments, simulations and applications. *Ph.D. thesis*, University of Kaiserslautern, 2013.
(18) Kahl, P.; Wall, S.; Witt, C.; Schneider, C.; Bayer, D.; Fischer, A.; Horn-von Hoegen, M.; Aeschlimann, M.; Meyer zu Heringdorf, F. Normal-incidence photoemission electron microscopy (NI-PEEM) for imaging surface plasmon polaritons. *Plasmonics* **2014**, *9*, 1401.
(19) Kahl, P.; Podbiel, D.; Schneider, C.; Makris, A.; Sindermann, S.; Witt, C.; Kilbane, D.; Horn-von Hoegen, M.; Aeschlimann, M.; Meyer zu Heringdorf, F. Direct observation of surface plasmon polariton



DOI: 10.1021/acsphotonics.8b01565
*ACS Photonics* 2019, 6, 600−604

propagation and interference by time-resolved imaging in normal-incidence two photon photoemission microscopy. *Plasmonics* **2018**, *13*, 239.

(20) Hecht, E. *Optik*; Oldenbourg, 2001.

(21) Meyer zu Heringdorf, F.-J.; Kahl, P.; Makris, A.; Sindermann, S.; Podbiel, D.; Horn-von Hoegen, M. Signatures of plasmoemission in two photon photoemission electron microscopy. *Proc. SPIE* **2015**, *9361*, 93610W−3.

(22) Meyer zu Heringdorf, F.-J.; Podbiel, D.; Raß, N.; Makris, A.; Buckanie, N. M.; Kahl, P. Spatio-temporal imaging of surface plasmon polaritons in two photon photoemission microscopy. *Proc. SPIE* **2016**, *9921*, 992110.

(23) Schmidt, O.; Bauer, M.; Wiemann, C.; Porath, R.; Scharte, M.; Andreyev, O.; Schönhense, G.; Aeschlimann, M. Time-resolved two photon photoemission electron microscopy. *Appl. Phys. B: Lasers Opt.* **2002**, *74*, 223.

(24) Kubo, A.; Onda, K.; Petek, H.; Sun, Z.; Jung, Y. S.; Kim, H. K. Femtosecond imaging of surface plasmon dynamics in a nanostructured Silver film. *Nano Lett.* **2005**, *5*, 1123−1127.

(25) Chelaru, L. I.; Meyer zu Heringdorf, F. J. In-situ monitoring of surface plasmons in single-crystalline Ag-nanowires. *Surf. Sci.* **2007**, *601*, 4541.

(26) Meyer zu Heringdorf, F. J.; Chelaru, L. I.; Möllenbeck, S.; Thien, D.; Horn-von Hoegen, M. Femtosecond photoemission microscopy. *Surf. Sci.* **2007**, *601*, 4700−4705.

(27) Lemke, C.; Leißner, T.; Evlyukhin, A.; Radke, J. W.; Klick, A.; Fiutowski, J.; Kjelstrup-Hansen, J.; Rubahn, H.-G.; Chichkov, B. N.; Reinhardt, C.; Bauer, M. The interplay between localized and propagating plasmonic excitations tracked in space and time. *Nano Lett.* **2014**, *14*, 2431−2435.

(28) Spektor, G.; Kilbane, D.; Mahro, A. K.; Frank, B.; Ristok, S.; Gal, L.; Kahl, P.; Podbiel, D.; Mathias, S.; Giessen, H.; Meyer zu Heringdorf, F.-J.; Orenstein, M.; Aeschlimann, M. Revealing the subfemtosecond dynamics of orbital angular momentum in nanoplasmonic vortices. *Science* **2017**, *355*, 1187−1191.

(29) Frank, B.; Kahl, P.; Podbiel, D.; Spektor, G.; Orenstein, M.; Fu, L.; Weiss, T.; Horn-von Hoegen, M.; Davis, T. J.; Meyer zu Heringdorf, F.-J.; Giessen, H. Short-range surface plasmonics: Localized electron emission dynamics from a 60-nm spot on an atomically flat single-crystalline gold surface. *Science Adv.* **2017**, *3*, No. e1700721.

(30) Radha, B.; Arif, M.; Datta, R.; Kundu, T. K.; Kulkarni, G. U. Movable Au microplates as fluorescence enhancing substrates for live cells. *Nano Res.* **2010**, *3*, 738−747.

(31) Podbiel, D.; Kahl, P.; Makris, A.; Sindermann, S.; Frank, B.; Davis, T. J.; Giessen, H.; Horn-von Hoegen, M.; Meyer zu Heringsdorf, F.-J. Imaging the nonlinear plasmoemission dynamics of electrons from strong plasmonic fields. *Nano Lett.* **2017**, *17*, 6569−6574.

(32) Podbiel, D.; Kahl, P.; Meyer zu Heringdorf, F. J. Analysis of the contrast in normal-incidence surface plasmon photoemission microscopy in a pump-probe experiment with adjustable polarization. *Appl. Phys. B: Lasers Opt.* **2016**, *122*, 90−6.

(33) Davis, T. J.; Frank, B.; Podbiel, D.; Kahl, P.; Meyer Zu Heringdorf, F.-J.; Giessen, H. Subfemtosecond and nanometer plasmon dynamics with photoelectron microscopy: Theory and efficient simulations. *ACS Photonics* **2017**, *4*, 2461−2469.



DOI: 10.1021/acsphotonics.8b01565
*ACS Photonics* 2019, 6, 600−604